CHALMERS
UNIVERSITY OF TECHNOLOGY

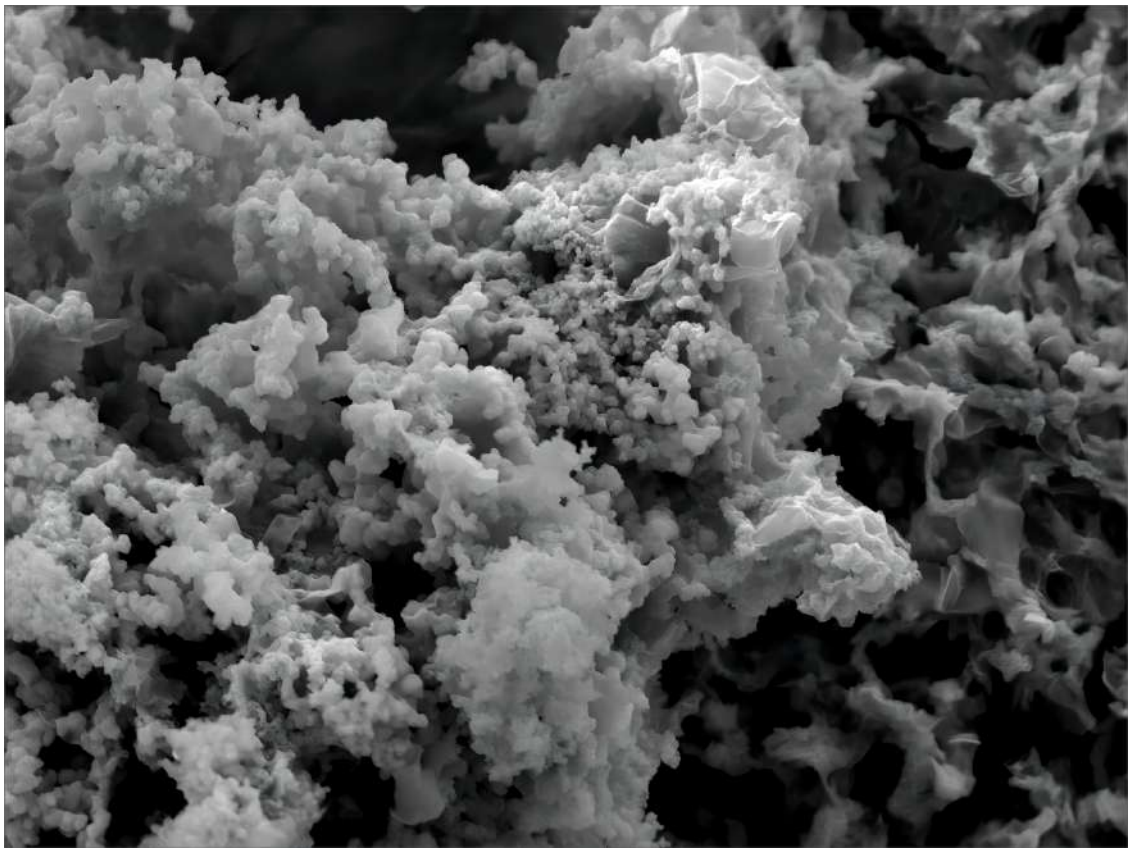

Electrochemical Co-deposition of Metal Oxide/Graphene Nanocomposites for Micro-supercapacitor

Master's thesis in Materials Engineering

JIAHAO SHI

DEPARTMENT OF INDUSTRIAL AND MATERIALS SCIENCE
CHALMERS UNIVERSITY OF TECHNOLOGY
Gothenburg, Sweden 2023
www.chalmers.se

Master's thesis 2023

Electrochemical Co-deposition of Metal Oxide/Graphene Nanocomposites for Micro-supercapacitor

JIAHAO SHI

CHALMERS
UNIVERSITY OF TECHNOLOGY

Department of Industrial and Materials Science
Division of Materials and Manufacture
Chalmers University of Technology
Gothenburg, Sweden 2023

Electrochemical Co-deposition of Metal Oxide/Graphene Nanocomposites for Micro-supercapacitor

JIAHAO SHI

Supervisor: Zhenyuan Xia, Department of Industrial and Materials Science
Examiner: Uta Klement, Department of Industrial and Materials Science

Master's Thesis 2023
Department of Industrial and Materials Science
Division of Materials and Manufacture
Chalmers University of Technology
SE-412 96 Gothenburg
Telephone +46 31 772 1000

Abstract

Micro-supercapacitors (MSCs) have gained significant attention in both academia and industry due to their excellent cycling stability, high power density, and long lifespan. They are widely used in miniaturized electrochemical energy storage devices and hold great potential for applications in portable electronics, wireless sensors, and other related fields. Efforts have been made to simplify the fabrication techniques of MSCs from the synthesis of electrode materials, electrode structure design, to the deposition process. However, there still lacks of a cost-effective and reliable manufacturing process to combine the multiple fabrication steps into a single operation. Hereby, this thesis work proposes an electrochemical co-deposition approach to make graphene and metal oxide nanocomposites layer in a single step to achieve high performance MSCs. Selective cathodic deposition was used to coat graphene-wrapped MnO_2 and Fe_2O_3 nanoparticles on target MSCs patterns. Various parameters, including the output signal, coating time, and concentration of metal salt precursor were examined to verify the optimal deposition condition. SEM, Raman, and XPS analyses were used to characterize the resulting hybrid materials. Additionally, the relative electrochemical performance of the MSCs devices with either liquid or solid electrolytes were evaluated. The result of this study offer an alternative approach for the one-step fabrication of graphene-related nanocomposites, specifically designed for miniaturized supercapacitors application.

Keywords: Graphene, micro-supercapacitor, metal oxide, electrochemical deposition.

Acknowledgements

Firstly, I would like to express my heartfelt gratitude to my supervisor, Zhenyuan Xia. He has taught me numerous laboratory techniques and skills, provided crucial advice for my research, and shown great care for both my academic and personal life. Secondly, I want to thank my examiner, Professor Uta Klement, for her valuable support throughout my master's thesis project. I am also grateful to all my colleagues in the laboratory: Ruiqi Chen, Zhaoyang Li, Sankar Sasidharan, James Randall, Keyvan Mirehbar, Tiance An, Xiaolong Li, and Karthik Jayakumar. I sincerely wish them all the best in their future endeavors. I would like to extend my gratitude to my two best friends and colleagues, Kaituo Zhang and Tianlin Zhang, for their assistance and support in both my personal and laboratory life. Special thanks go to my parents, Kai Shi and Xia Mu, and especially to my girlfriend, Hao Li, for their emotional support throughout my two-year master's program. Lastly, I want to express my appreciation to all the individuals who have provided assistance in various aspects of this thesis: Jessica Twedmark, Peter Hammersberg, Stefan Gustafsson, Antonio Mulone, and Charlott Ågren, Jiantong Li and his team.

Jiahao Shi, Gothenburg, Jun 2023

List of Acronyms

Below is the list of acronyms that have been used throughout this thesis listed in alphabetical order:

CV	Cyclic voltammetry
DCD	Direct current deposition
EGO	Electrochemically exfoliated Graphene Oxide
GCD	Galvanostatic charge-discharge
GIC	Graphite intercalation compounds
GO	Graphene oxide
IoT	Internet of Things
MC	Methyl cellulose
MSCs	Micro-supercapacitors
PCD	Pulse current deposition
PDDA	Poly(diallyldimethylammonium chloride)
SEM	Scanning Electron Microscopy
TMOs	Transition metal oxide
XPS	X-ray photoelectron spectroscopy

Contents

1
Introduction

1.1 Background

1.1.1 Internet of Things

The phrase "Internet of things" (IoT) refers to embedded devices that have Internet connectivity, enabling them to communicate with one another, with services, and with individuals on a global level. The emergence of the IoT concept stems from the increasing prevalence of Internet-enabled devices and the desire to connect them to create a more integrated and efficient system. By 2020, according to S. C. Mukhopadhyay et al.[1], there are 50 billions connected devices to IoT, which means that the average person in the world has more than six devices connected to the IoT. Thus, IoT is rapidly transforming our daily lives. Meanwhile, our daily lifes increasingly relying on IoT technology. The advancement of wireless technology within IoT has led to the significance of various IoT-based electronic devices like smartphones, smartwatches, and lightweight, flexible products. Within this realm, Micro-supercapacitors (MSCs) have emerged as a crucial electrochemical energy storage device. Offering rapid charging/discharging rates, high power density, and a long lifespan, MSCs hold great promise for IoT applications. Nevertheless, limitations in production processes and electrode material development currently prevent their widespread use as a power source for IoT devices.[2] [3]

1.1.2 Micro-supercapacitors (MSCs)

MSCs have garnered significant attention as energy storage devices in recent years due to their potential applications in microelectronics and portable devices. They essentially represent miniaturized versions of supercapacitors, intended for rapid energy storage and release, which is of great importance in numerous applications, such as sensors and implantable medical devices. Furthermore, MSCs possess a long cycle life, enabling multiple charge and discharge cycles without significant capacity loss.[4]

MSCs find wide-ranging applications, including wearable electronic products, implantable medical devices, and IoT devices. In wearable electronic products, MSCs can serve as power sources for sensors and displays, integrating into garments and accessories to enable portable charging. MSCs can also applied in medical cares. According to C.Gao et al.[5] , they developed a new kinds of MSCs that can be directly swallowed and can detect the body rapidly and painlessly. In implantable medical devices, MSCs can power sensors and stimulation devices, and they can

also be employed in drug delivery devices. In research of T.Wei et al.[6], a new kind of MSCs can be used for implant and it is self-degradable in human body. In IoT devices, MSCs can provide power to sensors and communication devices, while also serving as storage units for energy harvested from environmental sources like light and vibration.[7]

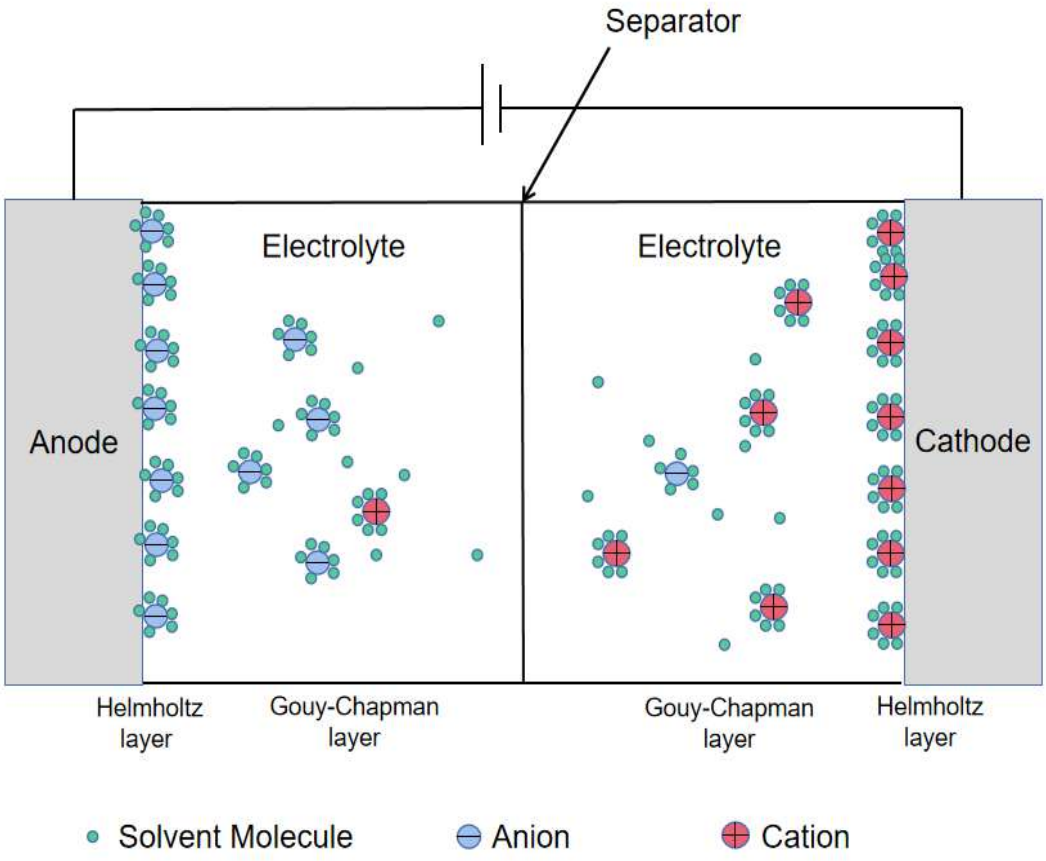

Figure 1.1: Mechanism of electrostatic double-layer capacitors.

1.1.3 Classification of Microsupercapacitors

1.1.3.1 Electrostatic double-layer capacitors (EDLCs)

Double-layer capacitors (EDLCs) are energy storage devices composed of two porous carbon electrodes separated by an electrolyte and a separator. The electrode materials used allow for a significant accumulation of charge at the interface between the electrode and the electrolyte. The creation of an electrical double layer of electrolyte ions on the surface of the conducting electrode is the primary process of supercapacitor storage.[8] The electrolyte contains ions capable of moving between the electrodes. The mechanism of EDLCs is shown in fig. 1.1.[9]
When a voltage is applied to the EDLCs, the ions in the electrolyte are attracted to the charged surfaces of the electrodes, forming two layers of ions, the Helmholtz layer and the Gouy-Chapman layer. The Helmholtz layer is a tightly packed layer

of ions close to the electrode surface, and the Gouy-Chapman layer is a more diffuse layer that extends further into the electrolyte. The combination of these two layers creates a high capacitance per unit volume, allowing EDLCs to store large amounts of electrical charge.[10]
The stored charge in the EDLCs can be discharged through an external circuit to deliver electrical power. The discharge process is reversible, allowing for the EDLCs to be charged and discharged many times without losing its capacity. The amount of energy that can be stored in the EDLCs is proportional to the capacitance and the square of the voltage.[11]
EDLCs have advantages over traditional batteries in that they can deliver high power in short bursts and have a long cycle life. However, they have a lower energy density and a higher self-discharge rate than batteries. EDLCs are promising technology for energy storage and can complement or replace traditional batteries in applications that require high power, such as in electric vehicles, renewable energy systems, and electronic devices.

1.1.3.2 Pseudo supercapacitors

Pseudo supercapacitors are a class of energy storage devices works on the principle of pseudocapacitance. Pseudo supercapacitors store energy by means of redox reactions occurring at the electrode-electrolyte interface, which results in a much higher capacitance compared to conventional capacitors, the mechanism of Pseudo supercapacitors is shown in fig. 1.2.[12][13]

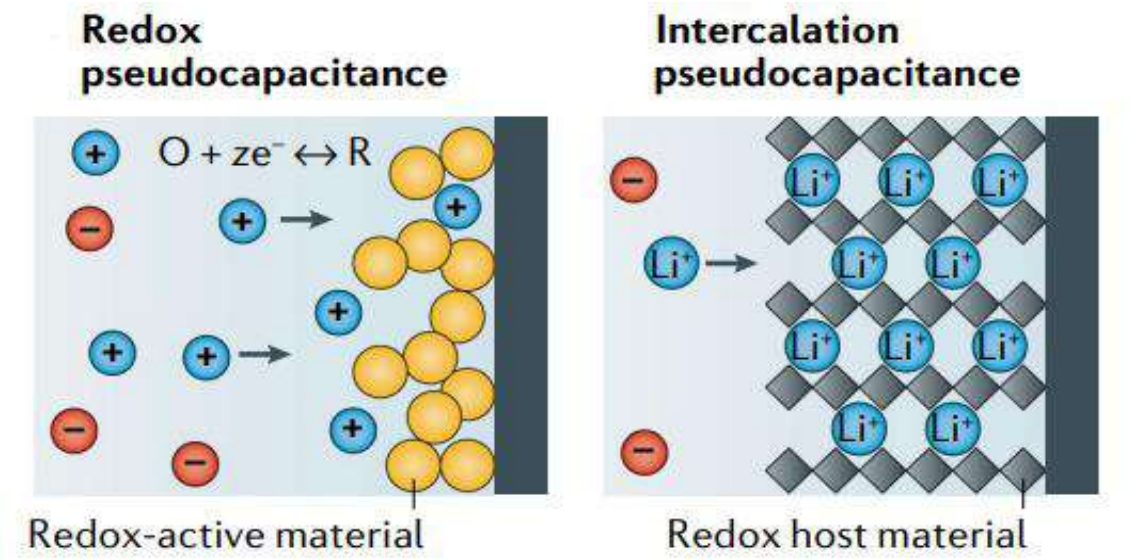

Figure 1.2: Mechanism of Pseudo supercapacitors. [12](open access)

The basic working principle of a Pseudo supercapacitor is based on the reversible faradaicreactions that take place at the electrode-electrolyte interface. The electrode materials in a Pseudo supercapacitor are typically transition metal oxides, such as ruthenium oxide, iridium oxide, and manganese oxide, which can undergo redox

reactions with the ions in the electrolyte. These redox reactions result in the formation and removal of surface-bound charges, leading to a change in the capacitance of the device.
The redox reactions that occur in Pseudo supercapacitors involve the transfer of electrons between the electrode and the electrolyte, resulting in the formation of charged species, such as ions or radicals, that are adsorbed onto the surface of the electrode. The charge storage capacity of Pseudo supercapacitors is determined by the specific surface area of the electrode and the type of redox-active species present in the electrode material.[13]

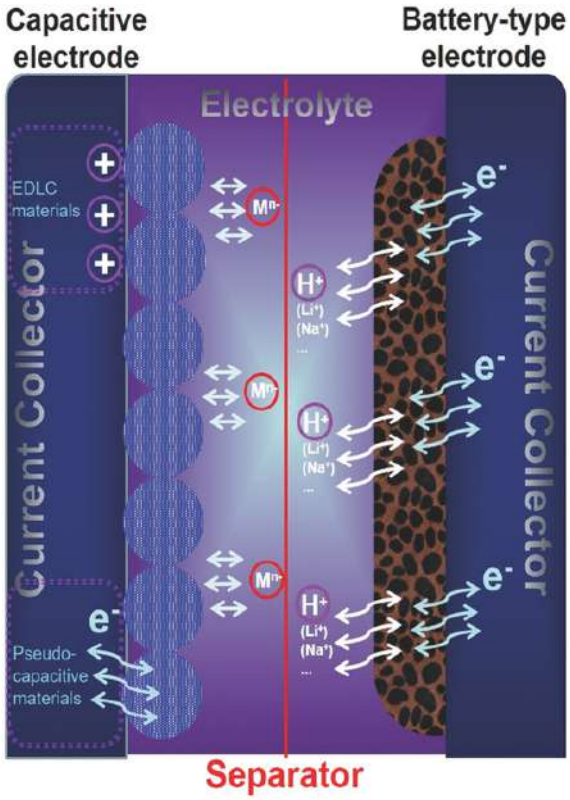

Figure 1.3: Mechanism of battery type supercapacitors.[14](open access)

1.1.3.3 Battery type supercapacitors

Battery-type supercapacitors, also known as hybrid capacitors or electrochemical capacitors, are a type of energy storage device that combines the characteristics of both batteries and capacitors. They have high energy density similar to batteries and high power density similar to capacitors. The mechanism of battery-type supercapacitors is shown in fig. 1.3.[14] involves both a reversible electrochemical reaction and phase changes at the interface between the electrode and electrolyte. In the electrochemical process, one electrode of the battery-type supercapacitor stores energy through Faradaic charge transfer, while the other electrode acts to maintain charge balance by adsorbing guest ions onto the surface of the active material.[15]

The electrodes of battery-type supercapacitors are mainly classified into two groups: 1) insertion-type of carbon-based materials, such as graphite and hard carbon; 2) conversion-type of transition metal oxides and hydroxide materials, such as Ni, Co and Mn based compounds. When a voltage is applied to the electrodes of a battery-type supercapacitor, the alkali ions (Li, Na) from the electrolyte intercalate into the electrodes through a reversible electrochemical reaction, resulting in a process known as battery-like charge storage.[14]
Battery-type supercapacitors are promising energy storage devices for a variety of applications, such as in hybrid electric vehicles, renewable energy systems, and portable electronics, due to their high energy and power density, long cycle life, and fast charging and discharging capability. However, the high cost and complexity of the electrochemical active electrolyte and the potential safety issues associated with lithium-ion batteries remain a challenge for the widespread use of battery-type supercapacitors.

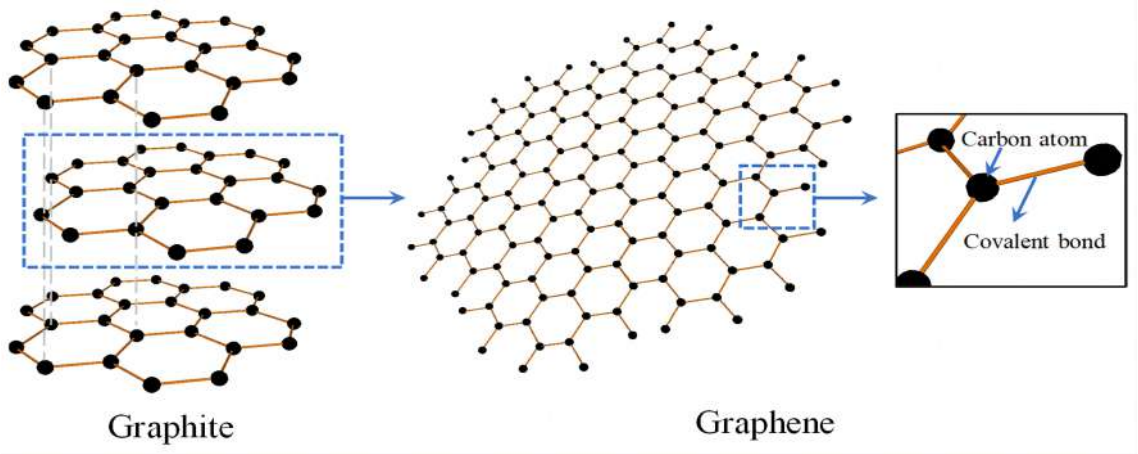

Figure 1.4: Structure of graphite and graphene.[16](open access)

1.2 Electrode materials

1.2.1 Graphene based 2D materials

Graphene is a 2D nanomaterial composed of carbon atoms arranged in a honeycomb structure resembling benzene rings. This unique structure results in numerous freely active electron clouds primarily derived from the p electron orbitals, vertically oriented within the 2D plane. Additionally, the exceptional stability of graphene ensures the smooth and unobstructed transmission of electrons, as they experience minimal hindrance or collisions with atomic nuclei. Consequently, graphene exhibits significantly higher electrical conductivity compared to conventional metals like copper, iron, and aluminum.[17] Meanwhile, It has many other unique properties, such as high mechanical strength and thermal conductivity. These properties make graphene a promising material for many applications, including MSCs.

Fig. 1.4 illustrates that graphite, a substance commonly encountered in daily life, is composed of multiple layers of graphene.[16] Graphene itself is a two-dimensional lattice structure consisting of tightly bonded carbon atoms arranged in a honeycomb pattern. The cohesion between adjacent layers is facilitated by weak van der Waals forces. When graphite is reduced to a single layer, it transforms into graphene, which is only one atom thick.

Graphene oxide (GO), in the form of single-layered sheets of carbon atoms that are fully oxidized, is another important type of graphene related 2D material. Numerous active edges and functional groups derived from oxygen are present in chemically altered GO. It is suitable for energy storage because it has good mechanical characteristics and good compatibility with other electrode materials.[18] However, GO itself is an insulating material, which limits its direct use as electrode materials in energy storage applications. Thus, further reduction treatment is necessary to fully recover the electric conductivity of GO.

Electrochemically exfoliated Graphene Oxide (EGO), is another derivative of graphene that is obtained by controllable electrochemical oxidation. This process introduces certain oxygen-containing functional groups, which leads to the formation of a hydrophilic and water-soluble material. Similar to GO, EGO is also derived from the exfoliation of graphite, consists of individual graphene sheets stacked together. In the production process, graphite undergoes intercalation and separation of carbon layers and the introduction of oxygen functional groups onto the sheet's surface. Consequently, graphite transforms into a hydrophilic and dispersible material, with each sheet being just one atom thick. However, the electrochemical process allows precise control over the intercalation and oxidation steps during the exfoliation, which results in moderately oxidized graphene sheets in comparison to fully oxidized GO by chemical exfoliation.

The large surface area of EGO allows for a large amount of charge to be stored on the surface, leading to high energy density. Meanwhile, the limited oxygen-containing functional groups on the surface of EGO also provide sites for charge storage, further increasing the capacitance of the material. All these advantages make EGO a good choice for electrode materials in supercapacitors.[19][20]

1.2.2 Transition metal oxide (TMOs)

Transition metal oxides (TMOs) are a class of materials that have attracted significant research interest due to their unique electronic, magnetic, and optical properties. Hence, TMOs have shown great potential for application in various fields, including energy storage devices such as supercapacitors. The high capacitance of TMOs can be attributed to their unique redox properties, which enable reversible charge storage through surface adsorption and faradaic reactions.

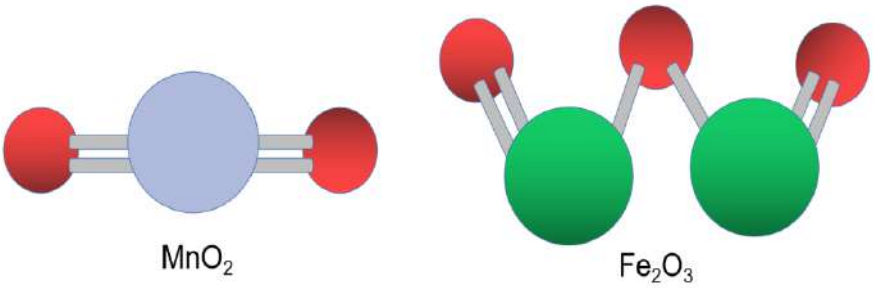

Figure 1.5: Ball-and-stick model of MnO_2 and Fe_2O_3.

Iron oxide (Fe_2O_3) and manganese oxide (MnO_2) are two TMOs that have received particular attention as electrode materials for supercapacitors. Iron is an earth-abundant material, and its relative oxide exhibits high theoretical capacitance and good cycling stability. Manganese oxide is also a promising electrode material due to its high specific capacitance and good electrical conductivity. Both Fe_2O_3 and MnO_2 can be easily synthesized using low-cost methods, such as sol-gel and hydrothermal techniques.
Fe_2O_3 and MnO_2 are being researched to develop the performance of supercapacitors. According to P Yang et al.[21], MnO_2 manowires and Fe_2O_3 nanotubes are used as electrode materials. It showed high energy density and outstanding stability over a wide potential window of 1.6 V. In Nilesh R. Chodankar's et al.[22] research, α-MnO_2 and α-Fe_2O_3 are used to fabricate thin film electrode for asymmetric supercapacitor. The product showed high specific capacitance of 145 $F{\cdot}g^{-1}$ with a high energy density of 41 $Wh{\cdot}\ kg^{-1}$ while maintaining a power density of 2.1 $kW{\cdot}\ kg^{-1}$.

1.3 Aim

The aim of this master thesis is to study how to apply graphene and metal oxide composite in energy storage devices. Use different equipment to analyze whether apply graphene and metal oxide composite can develop the morphology and performance of energy devices.

1.4 Approach

This study mainly focus on coating carbon based MSCs with manganese/iron oxide mixed with exfoliated graphene oxide, where manganese oxide is used on the positive electrode and iron oxide is used on the negative electrode. Scanning electron microscope (SEM), Energy-dispersive X-ray spectroscopy (EDS), Raman spectroscopy, and X-ray photoelectron spectroscopy (XPS) are used to analyze the morphology, elemental composition, chemical bonding and structure of coating layers. Cyclic Voltammetry (CV), Electrochemical Impedance Spectroscopy (EIS) and galvanostatic charge/ discharge (GCD) are used to test the electrochemical performance of the coated devices.

1.5 Limit

The main limitation of this study is that whether pulse deposition or direct deposition is adopted for the electrochemical deposition of Fe_2O_3, there is always visible peeling on the surface of the Fe_2O_3 electrode sample during annealing after the EPD is completed. This problem has not been solved during the course of this study.

2
Theory

2.1 Structure

Asymmetric supercapacitors (ASCs) utilize two distinct electroactive materials as the positive and negative electrodes, enabling the exploitation of two potential windows within a single cell, thereby increasing the overall energy density of the device. Transition metal oxides have been extensively researched for use in ASCs, as they can provide high specific capacitance by utilizing the rapid surface redox reactions of transition metal cations.[23]

2.2 Electrophoretic deposition (EPD)

Electrophoretic deposition (EPD) is a technique used to deposit charged particles or materials onto a conductive substrate under the influence of an electric field. This process is commonly used in the manufacturing of coatings, thin films, and other material structures. EPD is a versatile and cost-effective method for producing functional materials with tailored properties.

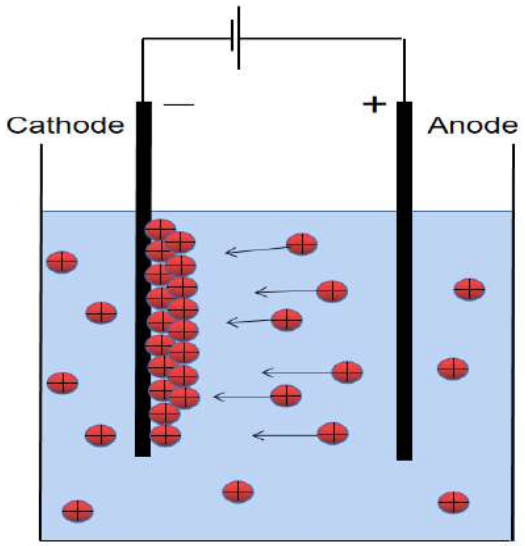

Figure 2.1: Mechanism of electrophoretic deposition.

The electrophoretic deposition process involves suspending particles or materials in a liquid medium and applying an electric field across the medium. The materials

or particles that are charged go in the direction of the electrode that is negatively charged and deposit there. By altering the electric field strength, timing, and other factors, the deposition process may be managed. EPD has several advantages over other deposition techniques, including the ability to coat complex geometries and the ability to control the thickness and morphology of the deposited material. The mechanism of EPD is shown in Figure 2.1. According to the figure, when an energy source is applied, positively charged particless will gathered on the cathode and form thin film. The EPD process allows for the deposition of a high surface area electrode material with excellent electrical conductivity, which is essential for achieving high power and energy density in MSCs. [24]
There are two types of EPD methods used in this study. The first one is direct current deposition (DCD), also known as continuous deposition, is a technique that involves a continuous flow of precursor material to deposit thin films onto a substrate. Direct deposition provides high deposition rates and simplicity of operation, favoring large-scale manufacturing applications. The second one is pulse current deposition (PCD), which utilizes intermittent pulses of the precursor material to achieve thin film growth. The process involves injecting precursor molecules or ions into a deposition chamber, followed by a pulse of energy to initiate surface reactions and promote film growth. Apart from normal settings, as shown in Figure 2.1, When using PCD, a control signal should also be applied. In this way, PCD enables precise control over film properties, composition, and thickness, making it ideal for tailored films and complex structures.
The following equations can be used to describe the electrosynthesis and deposition process of metal oxide (MO_x) using the cathodic approach[25]:

$$NO3^- + H_2O + 2e^- \longrightarrow NO2^- + 2OH^- \tag{2.1}$$

$$Mn^{2+} + 2OH^- \longrightarrow Mn(OH)_2 \tag{2.2}$$

$$Mn(OH)_2 \longrightarrow MnO_2 + 2H^+ + 2e^- \tag{2.3}$$

The three steps in the proposed mechanism for cathodic deposition of manganese oxide are as follows: (1) When potential is applied to the electrolytic cell, the reduction of nitrate ions take place and hydroxyl ions are formed.(2) Then those hydroxyl ions combined with manganese ions and form $Mn(OH)_2$; (3) in the final step, further oxidation of the adsorbed manganese hydroxide to MnO_2 with the release of a proton during the thermal annealing process.

3
Methods

3.1 Experiment

All of the MSCs used in this study is prepared by Jiantong Li's team from Sveriges största tekniska universitet (KTH), fig. 3.1 shows the appearance of MSCs.

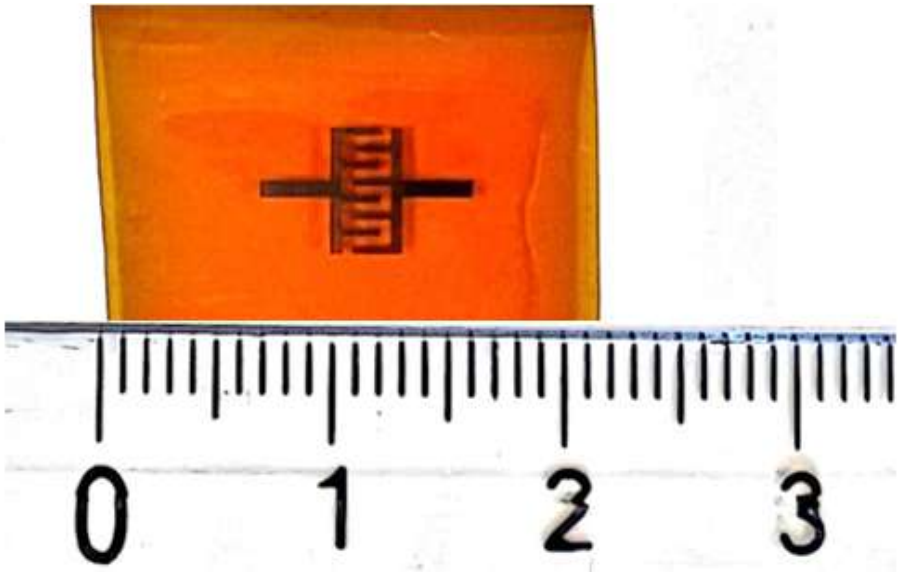

Figure 3.1: Photo of MSCs provided by JianTong Li's team from KTH.

3.1.1 Electrochemically exfoliated Graphene Oxide(EGO) Preparation

Intercalation of graphite is the first step to prepare exfoliated graphene oxide. During intercalation, graphite intercalation compounds (GIC) will be formed. In his process, graphite is used as the anode and immersed in an electrolyte, platinum is used as the cathode.
Electrolyte is prepared by dissolving 6.122g of sodium perchlorate in 50ml dimethyl carbonate/propylene carbonate organic solvent. The ratio of dimethyl carbonate and propylene carbonate is 4:1. Then, a graphite foil is cut into 2.5x2.5cm, which is the same size as platinum electrode. Bio-Logic SP-300 station is used to apply voltage to the intercalation system. An applied voltage of 10V was set on the EC-lab

software during the intercalation. After 30 minutes of intercalation, switch off the process and remove the intercalated graphite foil as well as platinum electrode from the electrolyte.

When graphite is used as the positive electrode, oxidation occurs, causing carbon atoms to lose electrons. This creates a favorable environment for perchlorate ions to intercalate between the graphite layers and maintain charge balance. At the cathode, platinum facilitates the reduction of sodium ions present in the electrolyte to elemental sodium, as the electrons depart from the graphite.

The second step is exfoliation of graphite intercalation compounds. In this process, GIC and platinum electrode is assembled in the same way as intercalation. But the electrolyte is changed to Ammonium sulfate, 1mol/L. After 6.607g of $(NH_4)_2SO_4$ is dissolved in water, pH test strips are used to detect the acidity of the electrolyte, which is generally pH 3-4. During exfoliation, the voltage start from 5V, and slowly changed from 5V to 10V. The limits of current is 2A. When the voltage is added to 10V, wait for the GIC piece to break on its own or for the current to drop to 0A, which means the exfoliation is stopped. EGO form on the top of the electrolyte. By vacuum filtration with water and ethanol, remaining salts and electrolyte can be removed and EGO can be collected.

The EGO collected is dispersed into a solvent mixture consisting of 50% water and 50% ethanol. To improve the dispersion stability, 0.25ml of 10wt% Poly(diallyl dimethyl ammonium chloride) (PDDA) is added into the EGO dispersion. Then, the dispersion subjected to overnight sonication. After that, the dispersion is treated by centrifugation at 1500 rpm and 0 degree Celsius for 10 minutes. During this process, large piece of less exfoliated graphite is removed from the product and precipitate at the bottom of the test tube. After centrifuge, the precipitate at the bottom is carefully removed to obtain the final EGO suspension, which is shown in fig. 3.2.

Figure 3.2: EGO achieved by electrochemical preparation.

3.1.2 Precursor Preparation

The precursor used for depositing on anode is prepared by mixing 51mg Manganese nitrate ($Mn(NO_3)_2 \cdot 4H_2O$) with 10ml EGO and 5mg Methyl cellulose (MC). The concentration of Manganese nitrate is 0.02mol/L. The cathode precursor is consist of Iron(III) nitrate ($FeN_3O_9 \cdot 9H_2O$) with EGO and MC. Same as anode precursor, the concentration of Iron nitrate is 0.02mol/L.

3.1.3 Electrophoretic deposition (EPD)

During this study, two kinds of electrophoretic deposition methods are applied, called direct current deposition (DCD) and pulse current deposition (PCD).

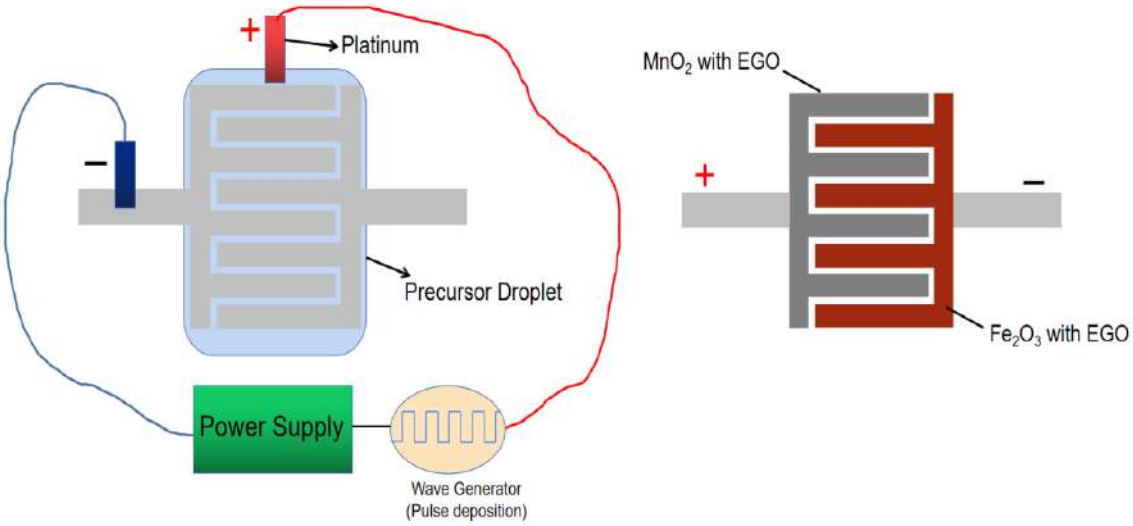

Figure 3.3: The process of electrophoretic deposition.

Table 3.1: Parameters of Electrophoretic deposition process

Precursor	Deposition method	Time/min
$Mn(NO_3)_2$ with EGO and MC	DCD	5
$Mn(NO_3)_2$ with EGO and MC	PCD	10
$Mn(NO_3)_2$ with EGO and MC	PCD	20
$Mn(NO_3)_2$ with EGO and MC	DCD	2.5
$Mn(NO_3)_2$ with EGO and MC	DCD	5
$Mn(NO_3)_2$ with EGO and MC	DCD	10
$Fe(NO_3)_3$ with EGO and MC	PCD	20
$Fe(NO_3)_3$ with EGO and MC	PCD	40
$Fe(NO_3)_3$ with EGO and MC	PCD	80
$Fe(NO_3)_3$ with EGO and MC	DCD	10
$Fe(NO_3)_3$ with EGO and MC	DCD	20
$Fe(NO_3)_3$ with EGO and MC	DCD	40

As shown in the fig. 3.3, the precursor solution is first dropped on the supercapacitor substrate. Feel free to pick one of the electrodes of the supercapacitor to connect to the cathode. The platinum electrode is connected to the anode and comes into contact with the precursor solution droplet. If PCD is used, it is also necessary to connect a wave generator in the circuit, which gives a pulse signal to the power supply. The potential of the power supply is set to 20 V and the current is limited to 0.5 mA. The specific time and method are shown in the table below. Since a pulse signal is applied to the power supply during PCD, the true working time of PCD is half that of DCD. Therefore, in order to compare which deposition method is better with the same true working time, the working time of PCD needs to be increased to twice that of DCD. After EPD process, anneal the coated supercapacitor in the vacuum oven under 100°C for 1h and 300°C for 1h. Then the final MSCs can be achieved and characterized.

3.2 Characterization

3.2.1 Morphology

3.2.1.1 Scanning electron microscopy (SEM)

Investigating the surface morphology of the EPD coated FeO_x/EGO and MnO_x/EGO thin films on MSCs was done using scanning electron microscopy (SEM). Using a JEOL JSM-7800F Prime at an acceleration voltage of 6 kV, images of the samples were captured. In addition to observing the samples in the vertical direction, the cross section was also observed in this study. the samples were immersed in liquid nitrogen for 1 min and the MSCs were cut in half with scissors and observed by SEM.

3.2.1.2 Raman spectroscopy

Raman spectroscopy is an analysis method that analyzes the scattering spectrum difference from the incident light frequency to obtain the molecular vibration and rotation. In this study, Raman spectroscopy called WITec alpha300 R is utilized to identify the molecular bonds, crystal structure and detect the chemical species of the coating layer on MSCs substrate.

3.2.1.3 X-ray Photoelectron Spectroscopy (XPS)

X-ray Photoelectron Spectroscopy (XPS) is a powerful analytical technique that enables the surface-sensitive investigation of elemental composition, chemical states, and bonding characteristics of materials. In this study, XPS is used to analyse the chemical states of Iron and Manganese to see whether the transition metal oxide deposited on the surface are Fe_2O_3 and MnO_2.

3.2.2 Electrochemical characterization

3.2.2.1 Cyclic Voltammetry (CV)

For every samples, Cyclic Voltammetry (CV) was conducted at a scanning rate of 5mV/s, 10mV/s ,20mV/s ,50mV/s and 100mV/s by using Bio-Logic SP-300 station.. When setting the parameter of the cell characteristics, electrode surface area are needed in order to calculate the current density. The surface area of the MSCs is measured by optical microscope as shown in the Figure 3.4. The surface area of the MSCs then can be calculated to be $0.147cm^2$.

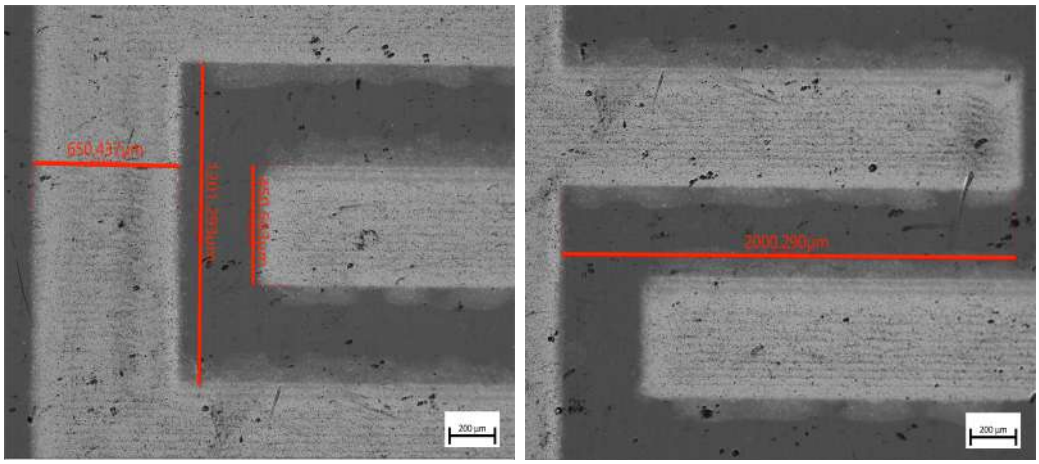

Figure 3.4: Optical microscopy for area calculation.

Then, the areal capacitance C_A was calculated by the following equation:

$$C_A = \int_0^{\triangle V} (I_C - I_D) dV / (2A\nu \triangle V) \tag{3.1}$$

Where I_C and I_D refers to charging and discharging currents; A is the working area of MSCs; $\triangle V$ is the Voltage range, from 0V-1.6V; ν is the scan rate.

3.2.2.2 Galvanostatic charge/ discharge (GCD)

Galvanic charge and discharge test were conducted between 0 and 1.6V at different current using Bio-Logic SP-300 station. Areal capacitance can also be calculated by using the following equation:

$$C_A = I \triangle t / A \triangle V \tag{3.2}$$

Where I is the charging current; $\triangle t$ is discharging time; A is working area of MSCs and $\triangle V$ is the voltage range, which is 0-1.6V.

4

Results

4.1 Morphology

Figure 4.1 shows the images of MnO_2 coating layers that have been deposited using the DCD (a, b, c) and PCD (d, e, f) methods. The visual examination reveals the surface of both samples displays the presence of cracks. A comparative analysis of these two methods reveals that, when observed under low magnification, the DCD-prepared MnO_2 coating layer appears smoother, much less cracks and contains fewer small particles on the surface compared to the PCD method. Furthermore, when examined at higher magnification, the DCD method displays a smaller grain size, while the PCD method exhibits a higher concentration of graphene oxide.

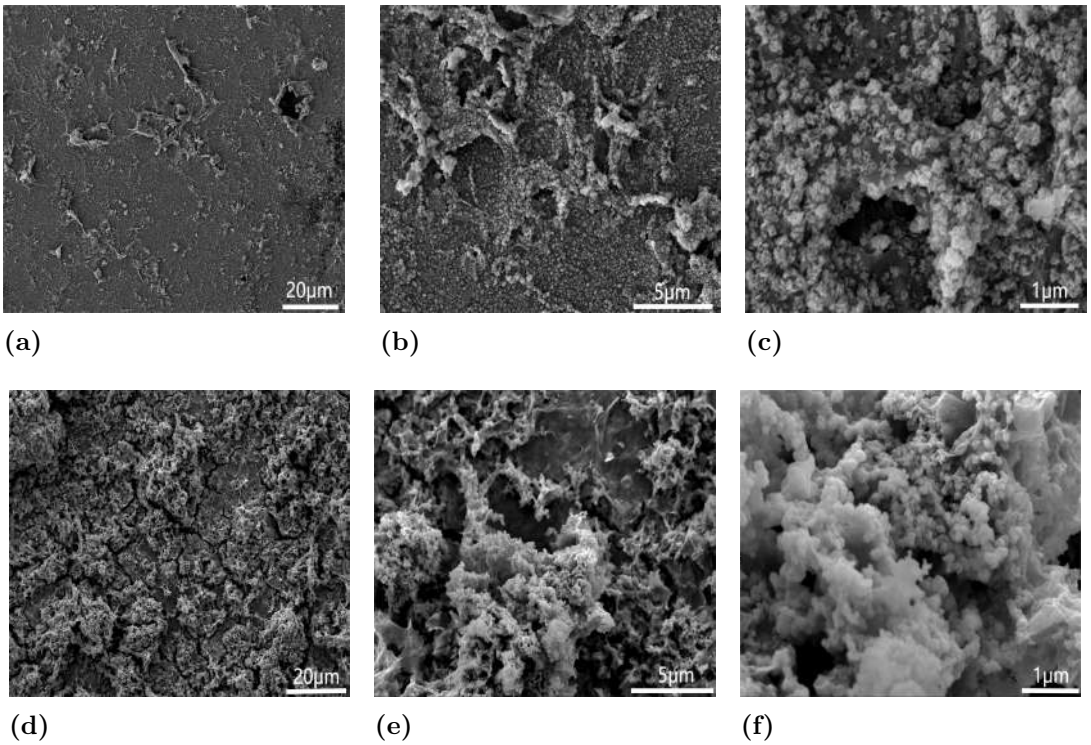

Figure 4.1: SEM images of MnO_2/EGO coatings on the MSCs (a)(b)(c) direct current deposition(t=5min) (d)(e)(f) pulse current deposition(t=10min).

Fe_2O_3 coating layers prepared by DCD (a, b, c) and PCD (d, e, f) are shown in

Figure 4.2.The analysis of Figure 4.2 (a) and (d) clearly demonstrates the presence of numerous cracks and defects on the surface of the sample produced using the DCD method. Moreover, the size of the cracks is so large that the entire coating layers are divided into many small island shapes. In contrast, the sample generated through the PCD method exhibits some defects, but overall, the surface appears remarkably hold in one piece. Upon closer inspection in Figure 4.2 (c)(f) at a higher magnification, it is evident that the grain shapes on the coating layer differ significantly between the DCD and PCD methods. Notably, the Fe_2O_3 particles on the DCD-prepared sample exhibit a flaky morphology, while those on the PCD-prepared sample display a predominantly flat shape. Furthermore, the Fe_2O_3 particles on the DCD-prepared sample adopt a flaky structure, whereas the Fe_2O_3 particles on the PCD-prepared sample resemble MnO_2 particles, mostly appearing blocky or spherical.

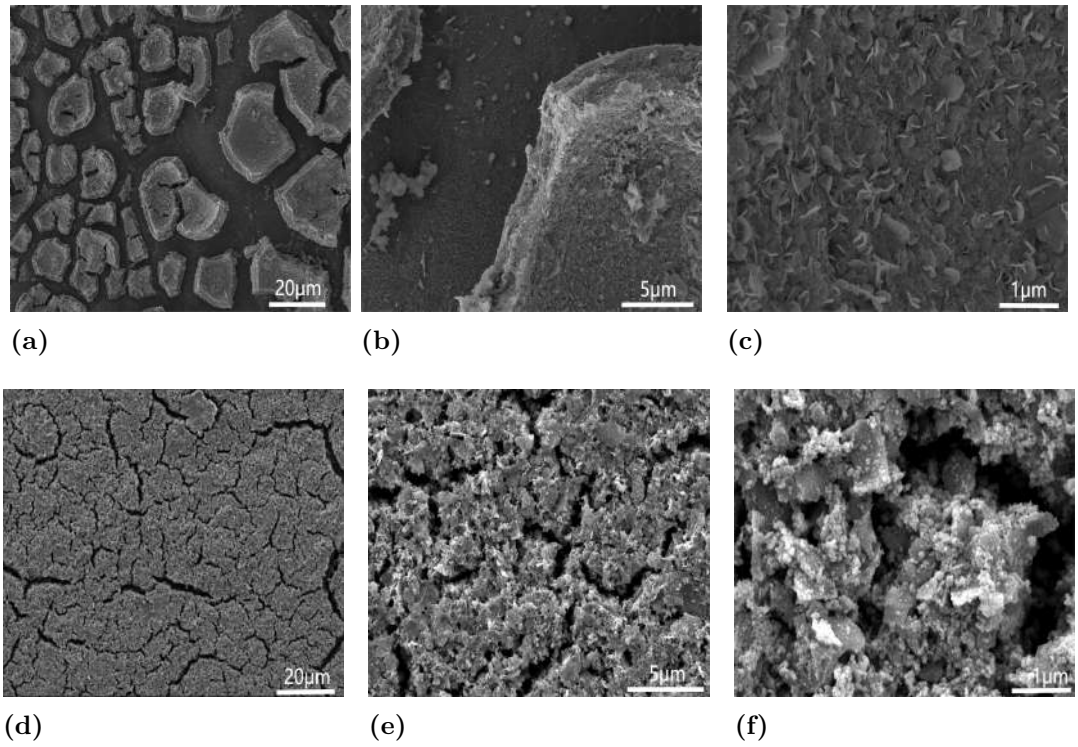

Figure 4.2: SEM images of Fe_2O_3/EGO coatings on the MSCs (a)(b)(c) direct current deposition(t=20min) (d)(e)(f) pulse current deposition(t=40min).

In addition to vertically analyzing the samples, this study also examined the cross-sectional view, as depicted in Figure 4.3, and measured the coating layer thickness for each parameter. A comparison between the PCD and DCD methods of plating MnO_2/EGO reveals that, under the same working time, the PCD method enables the plating of a thicker MnO_2/EGO layer. Specifically, the greatest thickness of PCD MnO_2 after 20 minutes is 6.516 μm. Regarding the plating of Fe_2O_3/EGO, no significant variation in the thickness of the coating layer is observed between PCD and DCD methods. Both of the highest thickness of PCD and DCD are around 2μm. Consequently, when combined with the prior SEM results in the vertical direction,

it can be concluded that PCD enhances the MnO_2/EGO loading and meanwhile provide a Fe_2O_3/EGO coating layer with fewer defects compared to DCD.

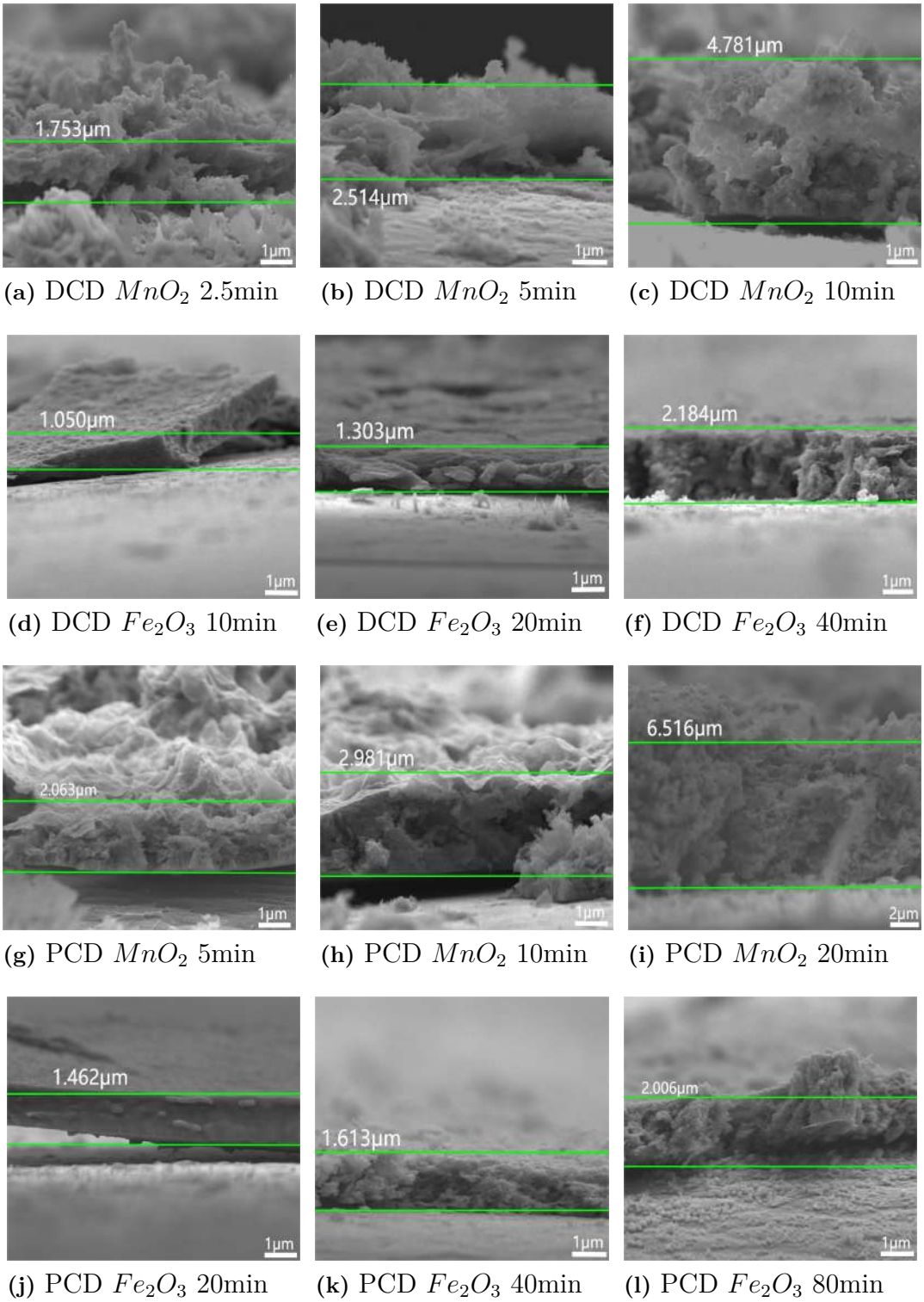

(a) DCD MnO_2 2.5min **(b)** DCD MnO_2 5min **(c)** DCD MnO_2 10min

(d) DCD Fe_2O_3 10min **(e)** DCD Fe_2O_3 20min **(f)** DCD Fe_2O_3 40min

(g) PCD MnO_2 5min **(h)** PCD MnO_2 10min **(i)** PCD MnO_2 20min

(j) PCD Fe_2O_3 20min **(k)** PCD Fe_2O_3 40min **(l)** PCD Fe_2O_3 80min

Figure 4.3: SEM images of cross section of samples prepared by all parameters.

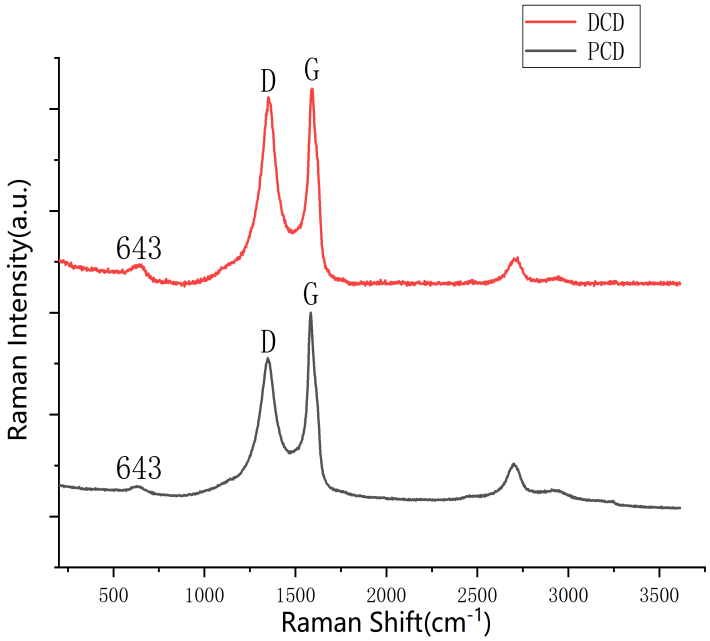

Figure 4.4: Raman spectroscopy of MnO_2 with EGO.

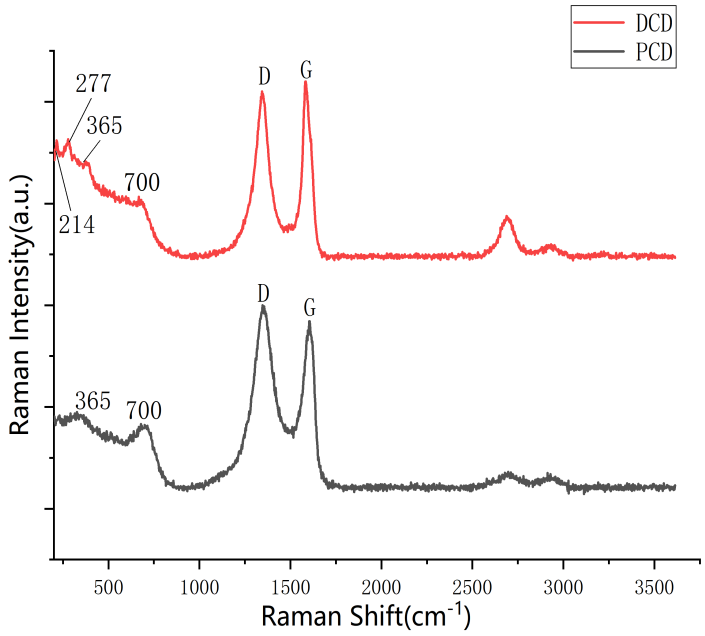

Figure 4.5: Raman spectroscopy of Fe_2O_3 with EGO.

Raman spectroscopy is used to compare the sample produced by PCD and DCD. The result of Raman spectroscopy is shown in Figure 4.3 and 4.4. In all PCD and DCD samples, two distinct peaks at 1352cm^{-1} and 1580cm^{-1} can be clearly observed, which refer to D peak and G peak.A secondary peak at approximately

2700 cm^{-1} corresponded to the 2D peak of graphene (the second harmonic of the D peak). The Raman spectrum in the low wavenumber range exhibited scattering peaks indicative of either MnO_2or Fe_2O_3 nanoflakes. In Raman spectroscopy of MnO_2 samples, a main peak at 643cm−1 is shown in Figure 4.4, which is identified as β-MnO_2 structure.[26] The (ID/IG) ratio of PCD is lower than DCD, which means that there are more defect in graphene prepared by DCD. In Raman spectroscopy of Fe_2O_3, in PCD, the main peak is around 365cm^{-1} and 700cm^{-1}, which correspond to T_{2g} (365cm^{-1}) and A_{1g} (700cm^{-1}). The nanoflakes of Fe_2O_3 consist of γ-Fe_2O_3 maghemite phase.[27] In DCD, apart from the same peak in PCD, two peaks in 214cm^{-1} and 277cm^{-1} can aslo be observed, which correspond to maghemite Fe_3O_4.[28] [29]Thus, two kinds of iron oxide are observed in DCD-prepared sample. By comparing the (ID/IG) ratio of two Fe_2O_3 samples, it is clear that the (ID/IG) ratio of PCD is higher than DCD, which means more defect in graphene prepared by PCD.

4.2 Chemical state and composition

X-ray photoelectron spectroscopy is uesd to test the chemical composition of DCD and PCD prepared samples.The parameters for the MnO2/EGO and Fe2O3/EGO samples fabricated using the DCD method were 5 minutes and 20 minutes, respectively;the parameters for the MnO2/EGO and Fe2O3/EGO samples prepared using the PCD method were 10 minutes and 40 minutes, respectively. All of the samples are tested by survey, C1s, O1s and Mn2p/Fe2p spectra. In Figure 4.5 (b) (c) and Figure 4.6 (b) (c), a main sp_2 peak can be observed at 286.4eV, which refers to C=C bond. Besides, other peaks at 285.8eV, 287.1eV and 288.8eV, which refers to C-OH, C-O and C=O components, respectively. The results of C1s spectra do not show any distinct difference between PCD and DCD. According to Figure 4.5(d) (e) and Figure 4.6 (d) (e), there are two main peaks at 530.2eV and 531.7eV, corresponding to M-O and MOH/C=O structure. The exist of these two kinds of bonding indicate that there are metal oxide and metal bonded with hydroxyl functional group.The presence of hydroxyl functional groups on the sample surface could be attributed to the adsorption of oxygen and water molecules. And other two peaks at 532.9eV and 533.9eV which refer to C-O and R-OH bonding. Figure 4.5 (f) and (g) shows the Mn2p spectrum of DCD and PCD prepared MnO_2 samples. Two peaks at 641.6eV for Mn $2p_{3/2}$ and 653.2eV for Mn $2p_{1/2}$. Meanwhile, Figure 4.6 (f) (g) show the chemical state of Fe 2p. A main peak at 710.8eV together with a shoulder peak at 713.3eV can be observed. Both of them refer to Fe $2p_{3/2}$. Fe(III) Oct. represent the iron ions in an octahedral coordination environment and Fe(III) Tet. represents for tetrahedral coordination of iron ions. Both of the samples exist a shake-up satellite at around 7eV higher than the main peak. It is attributed to multiplet splitting, which arises from the coupling of the core hole created during the photoemission process with the spin and orbital moments of the unpaired 3d electrons in the valence band.

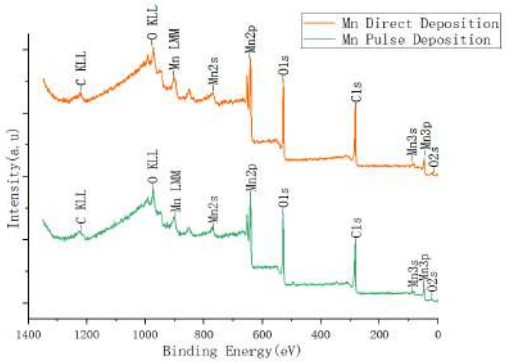

(a) Survey spectrum

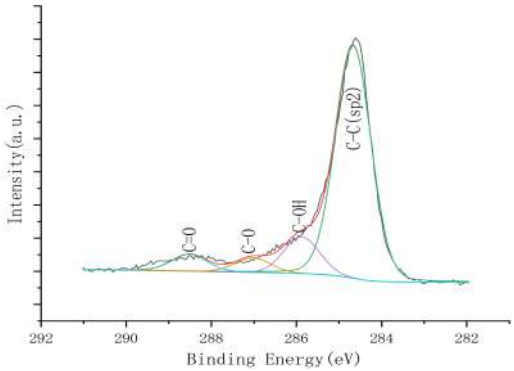

(b) DCD C1s

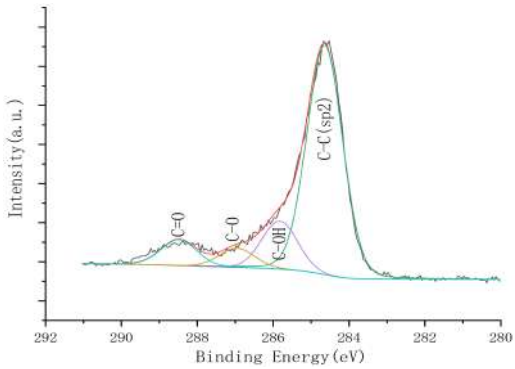

(c) PCD C1s

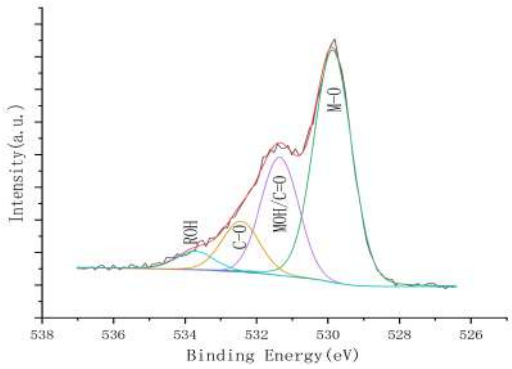

(d) DCD O1s

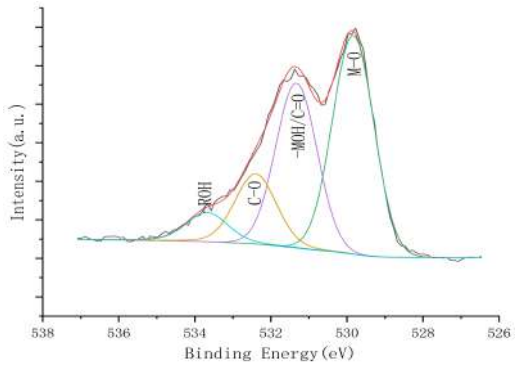

(e) PCD O1s

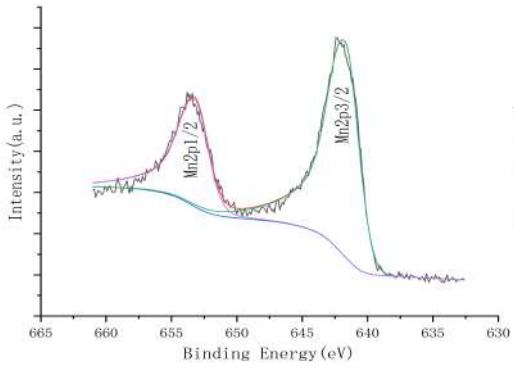

(f) DCD Mn 2p

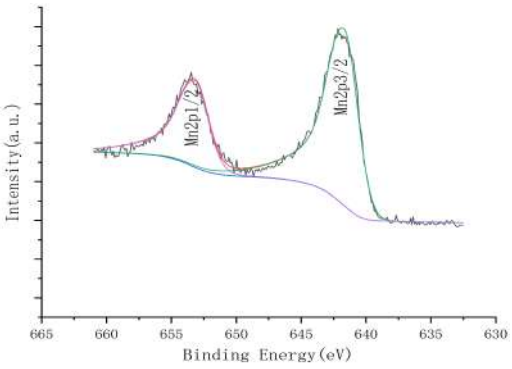

(g) PCD Mn 2p

Figure 4.6: XPS spectrum of MnO_2 with EGO.

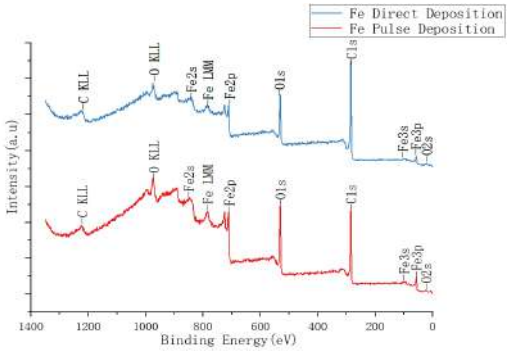

(a) Survey spectrum

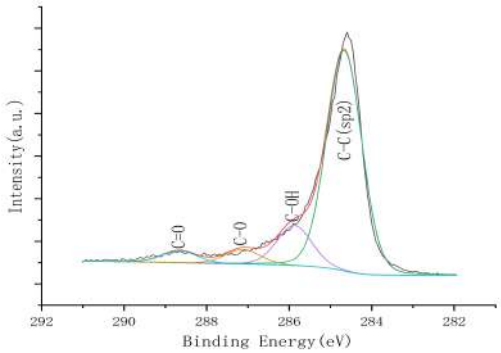

(b) DCD C1s

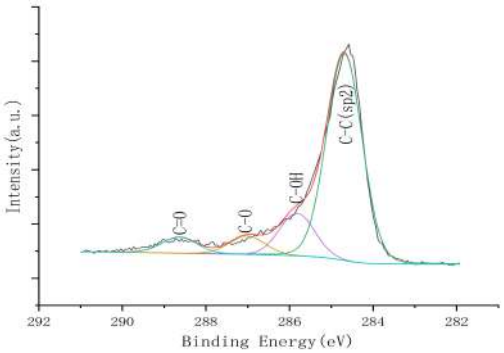

(c) PCD C1s

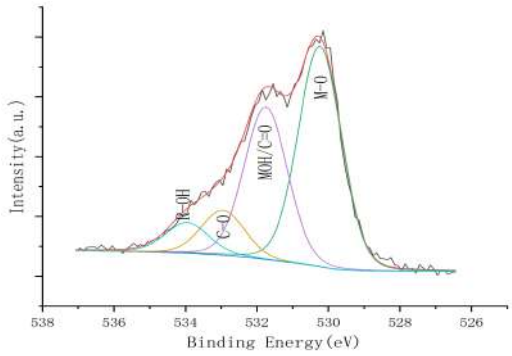

(d) DCD O1s

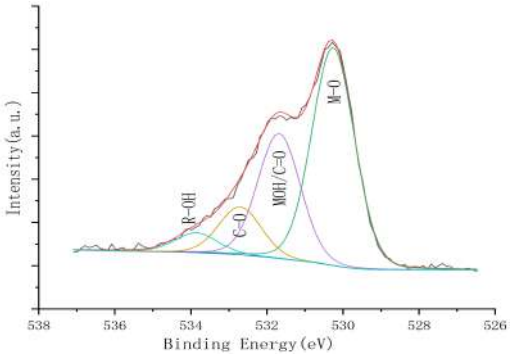

(e) PCD O1s

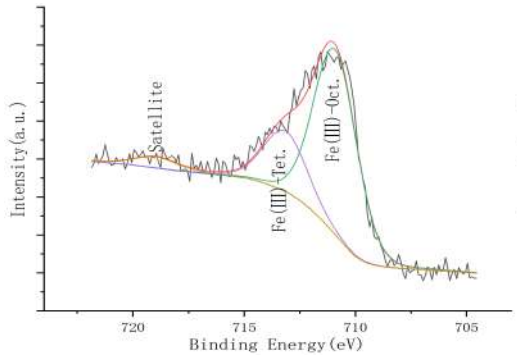

(f) DCD Fe 2p

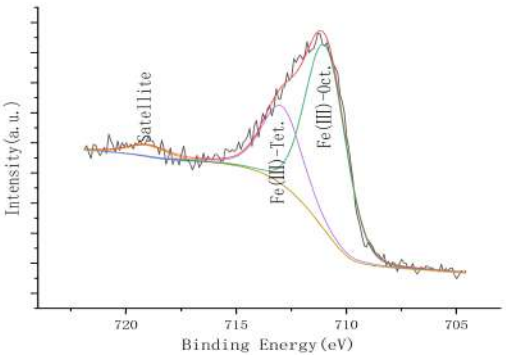

(g) PCD Fe 2p

Figure 4.7: XPS spectrum of Fe_2O_3 with EGO.

Table 4.1: Surface composition in atomic percent. (at.%)

Sample	Composition
Pulse deposition MnO_2 /EGO	C54.0% O34.0% Mn11.5% S0.5% Na<0.1%
Direct deposition MnO_2 /EGO	C49.5% O36.0% Mn14.5%
Pulse deposition Fe_2O_3/EGO	C58.0% O28.5% Fe13.5%
Direct deposition Fe_2O_3/EGO	C74.5% O19.0% Fe6.5%

By summarizing the results of XPS, surface composition and chemical state of all samples are shown in Table 4.1 and Table 4.2. The data in Table 4.1 reveals that the DCD MnO_2/EGO samples have higher concentrations of Mn and O compared to the PCD MnO_2/EGO samples. Conversely, the PCD MnO_2/EGO samples exhibit slightly higher levels of C. Similarly, the PCD Fe_2O_3 sample demonstrates significantly higher contents of Fe and O compared to the DCD Fe_2O_3 sample. Conversely, the DCD Fe_2O_3 sample has a higher C content. Based on table 4.2, it can be observed that in terms of chemical state, the DCD MnO_2/EGO sample exhibits higher content of M-O and Mn^{4+} at 20.0% and 14.5%, respectively, compared to the PCD MnO_2/EGO sample with 15.5% and 11.5%. Additionally, in the PCD Fe_2O_3/EGO sample, the content of M-O and Fe^{3+} is 15% and 13.5% respectively, whereas in the DCD Fe_2O_3/EGO sample, the content of M-O and Fe^3+ is only 9.5% and 6.5% respectively. This discrepancy can be attributed to the thicker coating layer achievable on MnO_2/EGO using the DCD method and on Fe_2O_3/EGO using the PCD method within the same processing time. Consequently, there will be an increased presence of metal and oxygen elements that only apper on the coating layer.

Table 4.2: Chemical state analysis in atomic percent. (at.%)

Binding energy (eV)	Bond type	PCD Mn	PCD Fe	DCD Mn	DCD Fe
284.6	C-C(sp^2)	38.5%	43.0%	38.5%	57.5%
285.8	C-OH	8.0%	8.5%	5.5%	10.5%
286.5	C-O	3.0%	3.5%	2.5%	3.5%
288.5	C=O	4.5%	3.5%	2.5%	3.5%
<530.0	M-O	15.5%	15.0%	20.0%	9.5%
531.5	M-OH/ C=O	11.5%	8.5%	9.5%	6.5%
532.5	C-O	5.0%	3.5%	4.5%	2.0%
>533.5	R-OH	2.0%	1.5%	2.0%	1.5%
641.7	Mn^{4+}	11.5%	-	14.5%	-
711.0	Fe^{3+}(Oct.)	-	9.0%	-	4.5%
713.0	Fe^{3+}(Tet.)	-	4.5%	-	2.0%

4.3 Electrochemical results

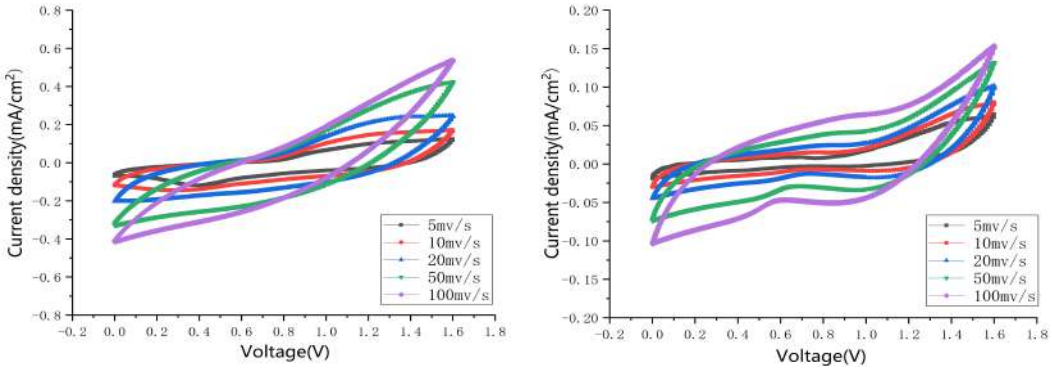

(a) DCD Mn2.5min Fe10min

(b) PCD Mn5min Fe20min

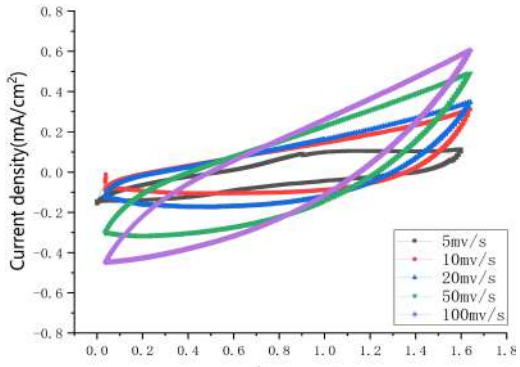

(c) DCD Mn5min Fe20min

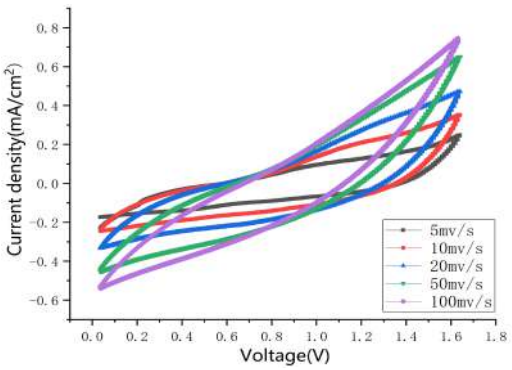

(d) PCD Mn10min Fe40min

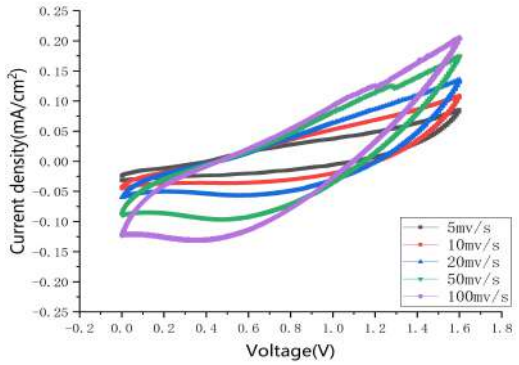

(e) DCD Mn10min Fe40min

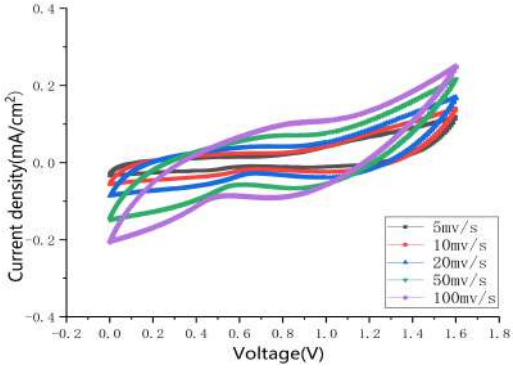

(f) PCD Mn20min Fe80min

Figure 4.8: The results of cyclic voltammetry.

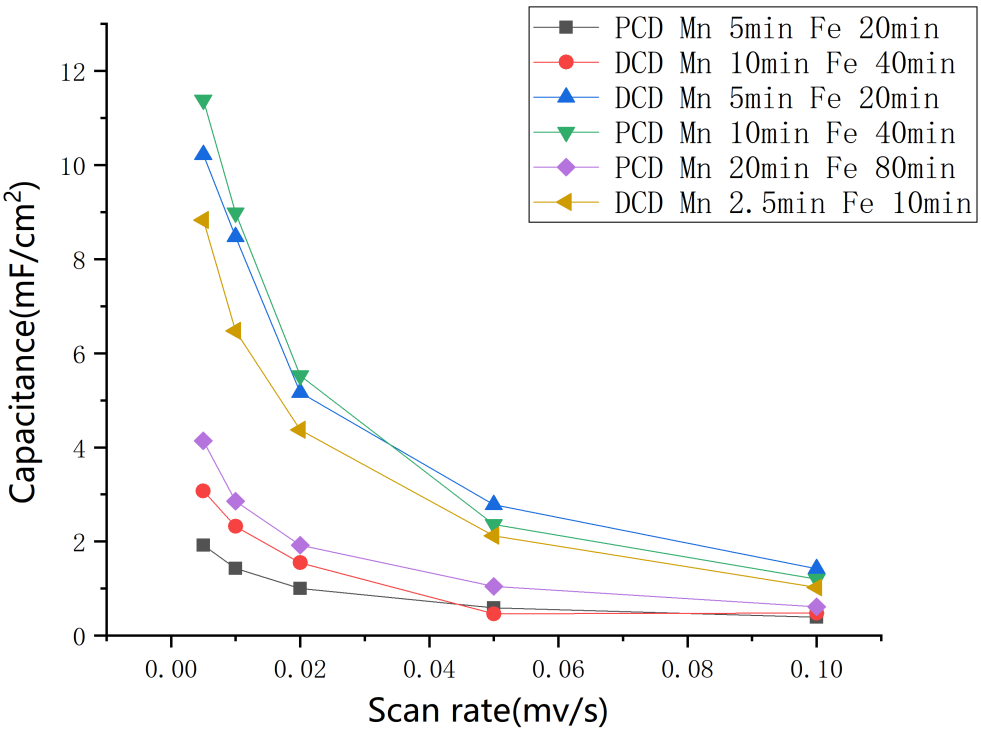

Figure 4.9: Capacitance of MSCs in all different parameters.

From the graph, it can be observed that the shapes of the CV curves resemble parallelograms at different scan rates, indicating fast and reversible redox reactions occurring at the electrodes during the test. Among them, it is evident that the current density range of PCD Mn10min Fe40min and DCD Mn5min Fe20 is significantly greater than that of the other parameter samples, approximately ranging from -0.5 to 0.7mA/cm^2.The cyclic voltammetry results of all the samples prepared for each parameter are shown in Figure 4.8. Each sample has corresponding curves at different scan rates: 5 mV/s, 10 mV/s, 20 mV/s, 50 mV/s, and 100 mV/s.

The capacitance of MSCs can be calculated using the method described in section 3.2.2.1, and the results are shown in Figure 4.9. Among samples with the same working time, PCD Mn10min Fe40min and DCD Mn5min Fe20min exhibit the highest capacitance. At a low scan rate of 5 mV/s, the capacitance of PCD Mn10min Fe40min is slightly higher, while at other scan rates, the capacitance of these two parameters is roughly the same. Furthermore, although DCD Mn2.5min Fe10min did not reach the capacitance of the aforementioned two parameters, it is significantly higher compared to the other parameters. It is approximately five times higher than that of PCD Mn5min Fe20min with the same working time. Finally, among the two groups with the longest working time, the capacitance of PCD is slightly higher than DCD, but there is still a difference compared to the three groups with the highest capacitance.

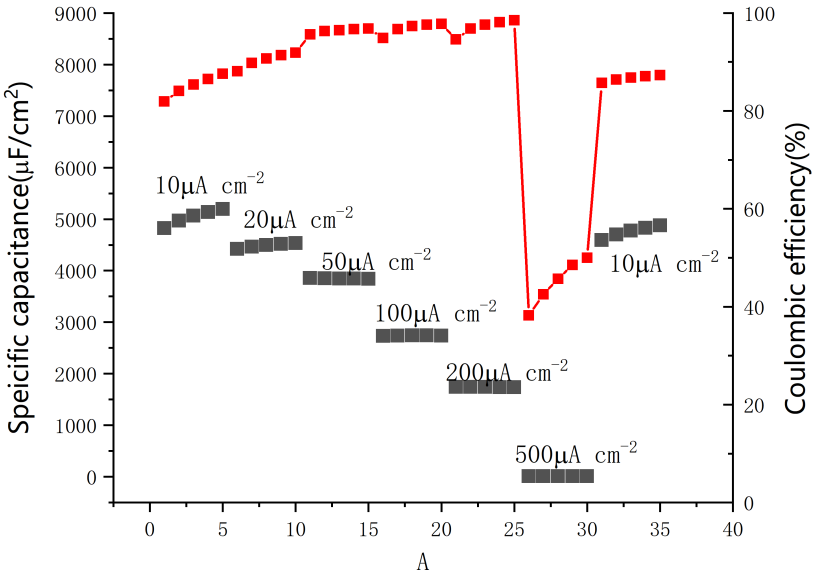

Figure 4.10: GCD result of DCD MnO_2/EGO 5min and Fe_2O_3/EGO 20min.

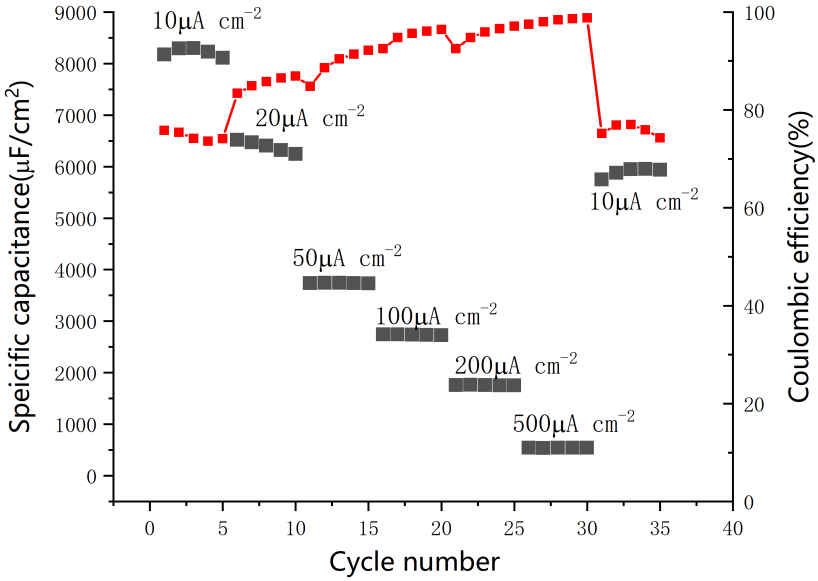

Figure 4.11: GCD result of PCD MnO_2/EGO 10min and Fe_2O_3/EGO 40min.

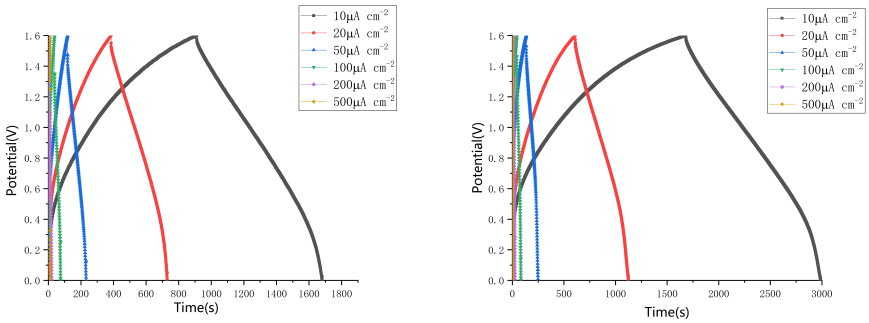

(a) DCD **(b)** PCD

Figure 4.12: Charge–discharge curves of MnO_2 and Fe_2O_3 at different current densities.

The GCD test results under different current densities ranging from 10 to 500 μA, as shown in Figure 4.12, exhibit triangular symmetric shapes, indicating the electrodes treated with MnO_2/EGO and Fe_2O_3/EGO possess favorable chemical properties. Figure 4.10 and 4.11 present the specific capacitance and coulombic efficiency of DCD Mn5min Fe20min and PCD Mn10min Fe40min at various current densities. In PCD Mn10min Fe40min, a high specific capacitance of 8.3 mF/cm^2 is achieved at 10 μA/cm^2, which is consistent with the results obtained from the CV test. Except for 10 μA/cm^2, the coulombic efficiency remains above 80% for all energy densities. In DCD Mn5min Fe20min, the maximum specific capacitance is 5.2 mF/cm^2, slightly lower compared to the results from the CV test. This could be attributed to an excessive number of defects on the Fe_2O_3 cathode surface under the DCD method, resulting in lower capacitance values in the GCD test compared to the CV test.

5
Conclusion

In summary, this study primarily investigated and evaluated the feasibility and effectiveness of two electrophoretic deposition (EPD) methods, namely pulse current deposition (PCD) and direct current deposition (DCD), for depositing MnO_2/Fe_2O_3 mixed with exfoliated graphene oxide (EGO) onto MSCs. The DCD method demonstrated excellent performance in depositing the MnO_2/EGO mixture, producing a smoother coating surface. However, DCD fell short in depositing the Fe_2O_3/EGO mixture, leading to the presence of numerous defects in the resulting Fe electrode. Furthermore, X-ray Photoelectron Spectroscopy (XPS) results revealed that, when using the DCD method for Fe deposition, a small amount of Fe_3O_4 formed on the sample surface in addition to the desired product Fe_2O_3. These factors have a certain impact on the overall performance of electronic devices, such as capacitance. The PCD method yielded similar results to DCD in depositing the MnO_2/EGO mixture, but PCD provided higher loading within the same working time. PCD demonstrated significant advantages over DCD in depositing the Fe_2O_3/EGO mixture. Cyclic Voltammetry (CV) and Galvanostatic charge/discharge (GCD) test results indicated that the electrochemical performance of PCD outperformed DCD in the two best-performing parameter sets. Observing the six parameter sets, it can be noted that DCD had a clear advantage at shorter working times, but as time increased, PCD gradually exhibited superior electrochemical performance.
Although both DCD and PCD effectively enhanced the performance of MSCs, further optimization is required for the treatment of the Fe cathode material. Regardless of whether DCD or PCD is used, the Fe electrode exhibited noticeable detachment after annealing, and there were also numerous defects observed under SEM examination. Therefore, the optimization of the Fe electrode is an essential part of future work.

Bibliography

[1] Subhas Chandra Mukhopadhyay and Nagender K Suryadevara. *Internet of things: Challenges and opportunities*. Springer, 2014.

[2] Jong-Hoon Lee, Guijun Yang, Choong-Hee Kim, Roop L Mahajan, Seul-Yi Lee, and Soo-Jin Park. "Flexible solid-state hybrid supercapacitors for the internet of everything (IoE)". In: *Energy & Environmental Science* 15.6 (2022), pp. 2233–2258.

[3] Christophe Lethien, Jean Le Bideau, and Thierry Brousse. "Challenges and prospects of 3D micro-supercapacitors for powering the internet of things". In: *Energy & Environmental Science* 12.1 (2019), pp. 96–115.

[4] Fan Bu, Weiwei Zhou, Yihan Xu, Yu Du, Cao Guan, and Wei Huang. "Recent developments of advanced micro-supercapacitors: Design, fabrication and applications". In: *npj Flexible Electronics* 4.1 (2020), p. 31.

[5] Chang Gao, Congcong Bai, Jian Gao, Yukun Xiao, Yuyang Han, Airam Shaista, Yang Zhao, and Liangti Qu. "A directly swallowable and ingestible micro-supercapacitor". In: *Journal of Materials Chemistry A* 8.7 (2020), pp. 4055–4061.

[6] Wei Tian et al. "Implantable and biodegradable micro-supercapacitor based on a superassembled three-dimensional network Zn@ PPy hybrid electrode". In: *ACS Applied Materials & Interfaces* 13.7 (2021), pp. 8285–8293.

[7] La Li, Zheng Lou, Di Chen, Kai Jiang, Wei Han, and Guozhen Shen. "Recent advances in flexible/stretchable supercapacitors for wearable electronics". In: *Small* 14.43 (2018), p. 1702829.

[8] Wen Yang, Mei Ni, Xin Ren, Yafen Tian, Ning Li, Yuefeng Su, and Xiaoling Zhang. "Graphene in supercapacitor applications". In: *Current Opinion in Colloid & Interface Science* 20.5-6 (2015), pp. 416–428.

[9] Jiři Libich, Josef Máca, Jiři Vondrák, Ondřej Čech, and Marie Sedlařıková. "Supercapacitors: Properties and applications". In: *Journal of Energy Storage* 17 (2018), pp. 224–227.

[10] Laurent Pilon, Hainan Wang, and Anna d'Entremont. "Recent advances in continuum modeling of interfacial and transport phenomena in electric double layer capacitors". In: *Journal of the Electrochemical Society* 162.5 (2015), A5158.

[11] Andrzej Lewandowski, Pawel Jakobczyk, Maciej Galinski, and Marcin Biegun. "Self-discharge of electrochemical double layer capacitors". In: *Physical Chemistry Chemical Physics* 15.22 (2013), pp. 8692–8699.

[12] Hammad Younes, Ding Lou, Md Mahfuzur Rahman, Daniel Choi, Haiping Hong, and Linda Zou. "Review on 2D MXene and graphene electrodes in

capacitive deionization". In: *Environmental Technology & Innovation* (2022), p. 102858.

[13] Y Liu, SP Jiang, and Z Shao. "Intercalation pseudocapacitance in electrochemical energy storage: recent advances in fundamental understanding and materials development". In: *Materials Today Advances* 7 (2020), p. 100072.

[14] Wenhua Zuo, Ruizhi Li, Cheng Zhou, Yuanyuan Li, Jianlong Xia, and Jinping Liu. "Battery-supercapacitor hybrid devices: recent progress and future prospects". In: *Advanced science* 4.7 (2017), p. 1600539.

[15] Huan Liu, Xuan Liu, Shulan Wang, Hua-Kun Liu, and Li Li. "Transition metal based battery-type electrodes in hybrid supercapacitors: A review". In: *Energy Storage Materials* 28 (2020), pp. 122–145.

[16] Houxuan Li, Ge Zhao, and Hong Zhang. "Recent Progress of Cement-Based Materials Modified by Graphene and Its Derivatives". In: *Materials* 16.10 (2023), p. 3783.

[17] Shuping Pang, Yenny Hernandez, Xinliang Feng, and Klaus Müllen. "Graphene as transparent electrode material for organic electronics". In: *Advanced Materials* 23.25 (2011), pp. 2779–2795.

[18] Prasanna Karthika, Natarajan Rajalakshmi, and Kaveripatnam S Dhathathreyan. "Functionalized exfoliated graphene oxide as supercapacitor electrodes". In: (2012).

[19] Shaikshavali Petnikota, Vadali VSS Srikanth, P Nithyadharseni, MV Reddy, S Adams, and BVR Chowdari. "Sustainable graphenothermal reduction chemistry to obtain MnO nanonetwork supported exfoliated graphene oxide composite and its electrochemical characteristics". In: *ACS Sustainable Chemistry & Engineering* 3.12 (2015), pp. 3205–3213.

[20] Yong Zhou, Qiaoliang Bao, Lena Ai Ling Tang, Yulin Zhong, and Kian Ping Loh. "Hydrothermal dehydration for the "green" reduction of exfoliated graphene oxide to graphene and demonstration of tunable optical limiting properties". In: *Chemistry of Materials* 21.13 (2009), pp. 2950–2956.

[21] Peihua Yang et al. "Low-cost high-performance solid-state asymmetric supercapacitors based on MnO2 nanowires and Fe2O3 nanotubes". In: *Nano letters* 14.2 (2014), pp. 731–736.

[22] Nilesh R Chodankar, Deepak P Dubal, Girish S Gund, and Chandrakant D Lokhande. "Bendable all-solid-state asymmetric supercapacitors based on MnO2 and Fe2O3 thin films". In: *Energy Technology* 3.6 (2015), pp. 625–631.

[23] Nitin Choudhary, Chao Li, Julian Moore, Narasimha Nagaiah, Lei Zhai, Yeonwoong Jung, and Jayan Thomas. "Asymmetric supercapacitor electrodes and devices". In: *Advanced Materials* 29.21 (2017), p. 1605336.

[24] Laxmidhar Besra and Meilin Liu. "A review on fundamentals and applications of electrophoretic deposition (EPD)". In: *Progress in materials science* 52.1 (2007), pp. 1–61.

[25] G Helen Annal Therese and P Vishnu Kamath. "Electrochemical synthesis of metal oxides and hydroxides". In: *Chemistry of materials* 12.5 (2000), pp. 1195–1204.

[26] Bosi Yin, Siwen Zhang, He Jiang, Fengyu Qu, and Xiang Wu. "Phase-controlled synthesis of polymorphic MnO 2 structures for electrochemical energy storage". In: *Journal of Materials Chemistry A* 3.10 (2015), pp. 5722–5729.

[27] Aaron M Jubb and Heather C Allen. "Vibrational spectroscopic characterization of hematite, maghemite, and magnetite thin films produced by vapor deposition". In: *ACS Applied Materials & Interfaces* 2.10 (2010), pp. 2804–2812.

[28] R Hatel, S El Majdoub, A Bakour, M Khenfouch, and M Baitoul. "Graphene oxide/Fe3O4 nanorods composite: Structural and Raman investigation". In: *Journal of Physics: Conference Series*. Vol. 1081. 1. IOP Publishing. 2018, p. 012006.

[29] R Yuvakkumar and Sun Ig Hong. "Green synthesis of spinel magnetite iron oxide nanoparticles". In: *Advanced Materials Research*. Vol. 1051. Trans Tech Publ. 2014, pp. 39–42.

DEPARTMENT OF SOME SUBJECT OR TECHNOLOGY
CHALMERS UNIVERSITY OF TECHNOLOGY
Gothenburg, Sweden
www.chalmers.se

CHALMERS
UNIVERSITY OF TECHNOLOGY